

Elastic and radiative π^+p scattering and properties of the Δ^{++} resonance

G. López Castro and A. Mariano

Departamento Física, Centro de Investigación y de Estudios Avanzados del IPN, Apdo. Postal 14-740, 07000 México, D.F., México

Abstract

We study the Δ^{++} contributions to elastic and radiative π^+p scattering within an effective Lagrangian model which incorporates the Δ , N , ρ and σ meson degrees of freedom. This model provides a description of the Δ resonance and its interactions that respects electromagnetic gauge invariance and invariance under contact transformations when finite width effects are incorporated. Following recent developments in the description of unstable gauge bosons, we use a complex mass scheme to introduce the finite width of the Δ^{++} without spoiling gauge invariance. The total cross section of elastic π^+p scattering, whose amplitude exhibits the resonant plus background structure of S -matrix theory, is used to fix the mass, width and strong coupling of the Δ resonance. The differential cross section of elastic scattering is found in very good agreement with experimental data. The magnetic dipole moment of the Δ^{++} , μ_Δ , is left as the only adjustable parameter in radiative π^+p scattering. From a fit to the most sensitive configurations for photon emission in this process, we obtain $\mu_\Delta = (6.14 \pm 0.51)e/2m_p$, in agreement with predictions based on the SU(6) quark model.

1. Introduction

According to the most recent compilation of the Particle Data Group [1], the properties of the overwhelming majority of baryonic resonances are badly known. Indeed, only conservative intervals are provided for most of the masses and widths of these resonances, either corresponding to the Breit-Wigner formula (with energy-dependent width) or to the pole position parameters [1]. Beyond masses and decay widths, other parameters characterizing baryonic resonances are even less known. In particular, a few determinations of the magnetic dipole moment (MDM) are provided only for the Δ^{++} resonance based on different approaches to radiative π^+p scattering [2, 3, 4, 5, 6]. Since the central values reported in these references spread over a wide range, the Particle Data Group [1] prefers to quote the interval $\mu_\Delta \sim 3.7$ to 7.5 (in units of nuclear magnetons $e/2m_p$) for the Δ^{++} MDM. In the present paper, we are seeking for a determination of this important property of the Δ^{++} in a full dynamical model which consistently describes elastic and radiative π^+p scattering.

The different determinations of the Δ^{++} MDM reported in [1] are based mainly on fits to the radiative π^+p scattering data of Refs. SIN [7] and UCLA [8] experiments (see also Refs. [9, 10]). Several inconsistencies or limitations can be pointed out among the different theoretical models used for this purpose. Some of these difficulties can be traced back to the set of Feynman rules used to describe the propagator and the vertices involving the Δ^{++} resonance. It is clear that any dynamical model used to describe the Δ resonance must satisfy general principles of quantum field theories such as gauge invariance and invariance under contact transformations. Electromagnetic gauge invariance is a fundamental property related to electric charge conservation. Invariance under contact transformations ensures that irrelevant spin-1/2 degrees of freedom are removed from the physical spin-3/2 fields required to describe the Δ resonance [11]. Furthermore, we must be assured that these properties are not spoiled when the unstable character (finite width) of the resonance is taken into account. As it has been pointed out before, most of the current determinations of the Δ^{++} magnetic dipole moment [1] do not fulfill these general requirements.

In addition, the necessity of *ad hoc* form factors for vertices involving the Δ^{++} are usually advocated to achieve a better fit of the relevant experimental data. According to the philosophy of effective Lagrangian models, in the description of low-energy hadron interactions (as it is the case of elastic and radiative π^+p scattering in the Δ^{++} resonance region), we must incorporate only the (structureless) relevant degrees of freedom at that energy. Accordingly,

we expect form factors to play an important role only at higher energies. A typical example of such approach to the radiative π^+p scattering is provided by the non-relativistic isobar model used in Refs. [3].

Another kind of inconsistency has to do with the ambiguities related to invariance under contact transformations of Rarita-Schwinger fields $\psi^\mu(x)$. As is well known, the Feynman rules involving the propagator and vertices of the Δ^{++} depend upon an arbitrary parameter A [11]. This arbitrary parameter is the trace left in the Lagrangian of the model by the contact transformations (see Eq. (4)), which are required to remove spin-1/2 components from the Rarita-Schwinger field. Decay amplitudes calculated from the A -dependent Feynman rules should be, however, independent of A [11]. A common mistake in some calculations [12] is to take the simplest form of the propagator for the Δ^{++} corresponding to $A = -1$ (which drops its off-shell part) and, simultaneously, the vertex $\pi N\Delta$ for a different value of this parameter (for example $A = -1/3$). This inconsistency is also present in some determinations of the Δ^{++} MDM from A -dependent radiative π^+p scattering amplitudes, where it is used a specific value of this arbitrary parameter A as in the relativistic model of Ref. [2, 4]. The determination of the Δ^{++} MDM provided in Ref. [6] is free of these ambiguities related to contact transformations. Their method requires being able to detach the decay process $\Delta^{++} \rightarrow \pi^+p\gamma$ out of the whole radiative π^+p scattering amplitude [6]. However, resonances are non-perturbative phenomena associated to the pole of the S-matrix amplitude [13] and one can not detach them from its production or decay mechanisms.

A third approach currently used to determine the Δ^{++} MDM is based on the soft photon approximation [14]. In the approach of Ref. [5], the calculation of the radiative π^+p scattering amplitude up to terms of order zero in the photon energy ω_γ requires a specific ansatz for the off-shell elastic amplitude. Though some terms of order ω_γ^0 coming from the proton MDM are included [5], other terms in the amplitude corresponding to the four-particle vertices $\pi^+p\Delta^{++}\gamma$ (see Figs. 1(e-f) in Ref. [15]) are ignored. Furthermore, the finite width of the Δ^{++} which one expects to be important in the resonance region, are also ignored in Ref. [5]. One of the goals of the present paper (see also Ref. [16]) is to go beyond those approximations.

An important and new element of the present paper concerns the issue of gauge invariance of the amplitudes involving the Δ resonance when its unstable character (finite width) is taken into account. A consistent model of this charged resonance should provide amplitudes which are gauge-invariant by themselves instead of *imposing* this property to the

total amplitude. The search for a consistent description of resonances within quantum field theories has received much attention recently, with the advent of precise measurements of the Z^0 gauge boson properties at LEP [17]. In particular, it has been pointed out [17] that the naive introduction of the finite width effects in the Feynman rules involving the resonance can spoil gauge-invariance. Among the different methods proposed to cure problems associated to this gauge non-invariance in the case of gauge-bosons, the *fermion-loop scheme* [18] provides one of the simplest solutions. In the case of the W gauge boson, this approach implies that using a propagator and electromagnetic vertex of the W boson which includes the absorptive pieces of fermionic corrections allows to compute amplitudes that are gauge-invariant when finite width effects are present. Similar conclusions were drawn in Ref. [19] for the case of the ρ^\pm meson resonance.

The expressions for propagators and electromagnetic vertices of charged spin-1 resonances (for massless particles in loop corrections) can also be obtained by replacing the bare mass M_0^2 by $M^2 - iM\Gamma$ in the lowest order expressions for these Feynman rules. This so-called *complex mass scheme* offers a simple prescription to obtain gauge-invariant amplitudes when finite width effects are present. Based on the examples provided by the gauge boson and ρ meson resonances, in the present paper we will extend this prescription to the vertices and the propagator of the Δ^{++} resonance. We expect this rule would follow from the explicit computation of the (finite) absorptive corrections to the corresponding lowest order vertices of the Δ that involve πN loops (see Refs. [18, 19]). Our belief is based on the powerful constraint imposed by electromagnetic gauge invariance rather than on the specific dynamical model responsible for loop corrections to Green functions of the Δ^{++} .

The aim of the present paper is to determine the MDM of the Δ^{++} resonance by using a *full* dynamical model which consistently describes the data on elastic and radiative π^+p scattering. This model includes the Δ , N , ρ and σ meson degrees of freedom (see for example [20]). By fixing the free parameters (mass, width and coupling to π^+p of the Δ resonance) of the model from the total cross section of π^+p scattering in the resonance region, we are able to reproduce reasonably well the experimental data for the differential cross sections for elastic π^+p scattering. In addition, let us emphasize that the mass and width of the Δ^{++} required to fit the data on elastic π^+p scattering, are consistent with the Δ^{++} parameters defined from the pole position of the elastic amplitude. Our approach also provides an amplitude for radiative π^+p scattering that is gauge-invariant under electromagnetism when the finite width effects of the Δ^{++} resonance are taken into account. From the experimental

data about this process, we are able to determine the MDM of the Δ^{++} from the photon configurations that are more sensitive to this property.

Our paper is organized as follows. In sec. 2 we present the dynamical model which contains the degrees of freedom relevant for π^+p elastic scattering and discuss the procedure to introduce finite width effects in a consistent way. In sec. 3 we introduce electromagnetic interactions and compute the gauge-invariant Δ^{++} contribution to the amplitude of radiative π^+p scattering. In section 4 we determine the parameters of the Δ^{++} resonance from elastic and radiative π^+p scattering data. Finally our conclusions are given in sec. 5.

2. Elastic pion-proton scattering

In this section we introduce the interaction Lagrangians relevant for the description of πN elastic scattering. We also compute the Δ^{++} contribution to the amplitude of elastic π^+p scattering. A comparison with experimental data on the total and differential cross sections is deferred to section 4.1.

As is well known, the total cross section of π^+p scattering in the energy range $T_{lab} = 100 \sim 300$ MeV (T_{lab} denotes the kinetic energy of incident pions in the Lab system) exhibits a resonant behavior around $T_{lab} \approx 175$ MeV, corresponding to the production of the Δ^{++} , $(I, J) = (3/2, 3/2)$ resonance. The experimental cross section can contain also non-resonant background contributions which can either, be parametrized in terms of a softly-varying function around the resonance (see for example [15, 21]) or computed explicitly in a given dynamical model. In this paper we adopt the second approach.

For definiteness, let us write the expression of the total cross section for π^+p elastic scattering:

$$\begin{aligned} \sigma_T = & \frac{(2\pi)^4 m_N^2}{4|\vec{q} E(\vec{p}) - \vec{p} \omega(\vec{q})|} \int \frac{d\vec{q}'}{(2\pi)^3 \omega(\vec{q}')} \int \frac{d\vec{p}'}{(2\pi)^3 E(\vec{p}')} \delta^4(p + q - p' - q') \\ & \times \frac{1}{2} \sum_{ms', ms} |\mathcal{M}[\pi^+p \rightarrow \pi^+p](q', p', ms'; q, p, ms)|^2, \end{aligned} \quad (1)$$

where $q = (\omega, \vec{q})$, $p = (E, \vec{p})$ denote pion and proton four-momenta (primes refer to the same quantities in the final state), respectively, ms is the proton's spin projection, and $\mathcal{M}[\pi^+p \rightarrow \pi^+p]$ denotes the Lorentz-invariant scattering amplitude.

The dynamical model we advocate in this paper to compute the scattering amplitude involves nucleons, the $\Delta^{++}, 0$ resonances, the ρ and the σ meson degrees of freedom¹. The various pieces of the interaction Lagrangian density contributing to π^+p scattering are (see for example [20])² :

$$\hat{\mathcal{L}}_{hadr} = \hat{\mathcal{L}}_{\pi NN} + \hat{\mathcal{L}}_{\Delta\pi N} + \hat{\mathcal{L}}_{\rho NN} + \hat{\mathcal{L}}_{\rho\pi\pi} + \hat{\mathcal{L}}_{\sigma NN} + \hat{\mathcal{L}}_{\sigma\pi\pi} \quad (2)$$

where the individual terms are given by

$$\begin{aligned} \hat{\mathcal{L}}_{\pi NN}(x) &= -\left(\frac{f_{\pi NN}}{m_\pi}\right) \bar{\psi}(x) \gamma_5 \vec{\tau} \cdot (\partial \vec{\pi}(x)) \psi(x), \\ \hat{\mathcal{L}}_{\Delta\pi N}(x) &= \left(\frac{f_{\Delta\pi N}}{m_\pi}\right) \bar{\psi}_\Delta^\mu(x) \Lambda_{\mu\nu}(A) \vec{T}^\dagger \cdot (\partial^\nu \vec{\pi}(x)) \psi(x) + h.c., \\ \hat{\mathcal{L}}_{\rho NN}(x) &= -\frac{1}{2} g_\rho \bar{\psi}(x) \left[\gamma_\mu - \frac{\kappa_\rho}{2m_N} \sigma_{\mu\nu} \partial^\nu \right] \vec{\tau} \cdot \vec{\rho}^\mu(x) \psi(x), \\ \hat{\mathcal{L}}_{\rho\pi\pi}(x) &= -g_{\rho\pi\pi} \vec{\rho}_\mu(x) \cdot (\vec{\pi}(x) \wedge \partial^\mu \vec{\pi}(x)), \\ \hat{\mathcal{L}}_{\sigma NN}(x) &= g_{\sigma NN} \bar{\psi}(x) \psi(x) \sigma(x), \\ \hat{\mathcal{L}}_{\sigma\pi\pi}(x) &= \left(\frac{g_{\sigma\pi\pi}}{2m_\pi}\right) \sigma(x) (\partial_\mu \vec{\pi}(x)) \cdot (\partial^\mu \vec{\pi}(x)), \end{aligned} \quad (3)$$

and (A is an arbitrary parameter related to contact transformations to be defined below),

$$\Lambda_{\mu\nu}(A) = g_{\mu\nu} + \frac{1}{2}(1 + 3A)\gamma_\mu\gamma_\nu .$$

The isotopic fields $\psi(x)$ and $\psi_\Delta^\mu(x)$ denote the N and Δ baryons, respectively, while $\vec{\pi}(x)$, $\vec{\rho}^\mu(x)$ and $\sigma(x)$ denote the pion, ρ - and σ -meson fields. The arrow over the meson fields refers to the isospin space. \vec{T}^\dagger stands for the isospin 1/2 to 3/2 transition isospin operators, while $\vec{\tau}$ is used for Pauli isospin matrices. The constants $f_{\pi NN}$, $g_{\sigma NN}$, $f_{\Delta\pi N}$, $g_{\rho\pi\pi}$, and $g_{\sigma\pi\pi}$ denote the strong couplings among the different particles indicated as subindices, and $g_\rho = g_{\rho\pi\pi}(\kappa_\rho)$ is the vector (magnetic) coupling of the ρ -meson to the nucleon.

Note that $\hat{\mathcal{L}}_{\Delta\pi N}(x)$ in Eq.(3) is invariant under the contact transformation³:

$$\psi^\mu \rightarrow \psi^\mu + a\gamma^\mu\gamma_\alpha\psi^\alpha, \quad A \rightarrow A' = \frac{A - 2a}{1 + 4a}, \quad (4)$$

¹Throughout this paper we will assume isospin symmetry in the masses and strong couplings of hadrons.

²The Lagrangian densities corresponding to kinetic terms can be found for example in Ref. [15].

³The kinetic term for the spin-3/2 field and other interaction Lagrangians involving the $\psi^\mu(x)$ in Eq. (9) also remain invariant under this transformation (see ref. [11, 15]).

where $a \neq -1/4$ is an arbitrary parameter. Invariance under this transformation allows to eliminate irrelevant (spin-1/2) degrees of freedom in the ψ^μ field [11]. Physical scattering amplitudes should be independent of any particular choice of A in vertices and propagators involving the Δ baryon. As already advertised in the introduction, this fact is sometimes ignored in computing the Δ^{++} contribution to elastic and radiative π^+p scattering amplitudes (see for example Refs.[2, 4]).

In the present model, the elastic scattering amplitude is composed of several pieces:

$$\mathcal{M}(\pi^+p \rightarrow \pi^+p) = \sum_{i=\Delta^{++}, \Delta^0, n, \rho, \sigma} \mathcal{M}_i(\pi^+p \rightarrow \pi^+p) .$$

The contributions to the amplitude involving intermediate nucleon and Δ^0 baryons (in the crossed-channel) and the ρ and σ mesons (in the t -channel) are shown in Figure 1. They are expected to provide a smoothly-varying background term in the amplitude around the resonance region. The evaluation of these amplitudes from the interaction Lagrangians given above is straightforward. Therefore, we will focus now in the explicit form of the Δ^{++} contribution (resonance in the s -channel). As it was proven in Ref. [15], in the case of elastic and radiative π^+p scattering, the A -dependent Feynman rules involving the Δ can be replaced by a set of A -independent vertices and propagators called *reduced* Feynman rules. The calculation of π^+p scattering amplitudes using either set of rules, give rise to identical results [15]. The elastic scattering with the Δ^{++} intermediate state in the s -channel (see the first graph in Figure 1) is given by

$$\mathcal{M}_{\Delta^{++}}(\pi^+p \rightarrow \pi^+p) = -i \left(\frac{f_{\Delta\pi N}}{m_\pi} \right)^2 \bar{u}(p') q'_\mu G^{\mu\nu}(p+q) q_\nu u(p), \quad (5)$$

where $u(p) \equiv u(p, ms)$ denote proton spinors, and the reduced form of the Δ^{++} propagator is given by

$$G^{\mu\nu}(P) = \frac{i}{P^2 - m_\Delta^2} \left\{ (P + m_\Delta) \left[-g^{\mu\nu} + \frac{1}{3} \gamma^\mu \gamma^\nu + \frac{2}{3} \frac{P^\mu P^\nu}{m_\Delta^2} - \frac{1}{3} \frac{P^\mu \gamma^\nu - P^\nu \gamma^\mu}{m_\Delta} \right] - \frac{2}{3m_\Delta^2} (P^2 - m_\Delta^2) \left[(\gamma^\mu P^\nu - \gamma^\nu P^\mu) + (P + m_\Delta) \gamma^\mu \gamma^\nu \right] \right\}. \quad (6)$$

The elastic amplitude of Eq. (5) blows up when the total energy $\sqrt{P^2}$ approaches m_Δ . As is well known [1], this bad behavior can be cured naively by replacing $m_\Delta^2 \rightarrow m_\Delta^2 - im_\Delta \Gamma_\Delta$ in the denominator of the Δ^{++} propagator⁴(Γ_Δ is the decay width of the Δ). However, as

⁴The finite widths of the Δ^0 baryon and the ρ , σ mesons do not play any role since these resonances do not appear in the s -channel.

it has been widely discussed elsewhere [18], this prescription breaks gauge invariance when photons are attached to all charged particles of the elastic scattering (see the first row in Figure 2) to produce the corresponding radiative decay amplitude.

The simplest solution to maintain gauge invariance in the radiative π^+p scattering amplitude when finite width effects are incorporated, is to replace $m_\Delta^2 \rightarrow m_\Delta^2 - im_\Delta\Gamma_\Delta$ in *all* the Feynman rules involving the Δ^{++} resonance [15] (this is the so-called complex mass scheme). As it has been explained in the introduction, this prescription is well justified for the amplitudes involving intermediate Z^0 and W^\pm gauge boson [22, 23] and the ρ^\pm meson resonances [19]. This is a rigorous result obtained when one-loop absorptive corrections are included in the propagator and the electromagnetic vertex of the charged resonance, with massless particles running in loops [18, 19]. Thus, in the present case we will use the complex mass scheme as a useful *prescription* to obtain gauge-invariant amplitudes. As in the case of spin-1 charged resonances, we expect that absorptive pieces of π^+p loop corrections to the $\Delta^{++} \rightarrow \gamma\Delta^{++}$ vertex and the Δ^{++} propagator would generate these results in the limit of massless pions and protons. Since this limit may be questionable, let us point out that a Laurent expansion of the amplitude (with Dyson summation of the Δ^{++} self-energy corrections) around the pole will give similar results to the complex mass scheme, with regular terms being absorbed into background contributions (see for example Refs. [15, 17, 22]).

3. Radiative pion-proton scattering

In this section we focus on the calculation of the gauge-invariant $\pi^+p \rightarrow \pi^+p\gamma$ scattering amplitude in the presence of the Δ^{++} finite width effects. Comparison with experimental data on energy and angular photon distributions is left to section 4.2.

For definiteness, let us start with the expression for the differential cross section of this process:

$$\begin{aligned} \frac{d\sigma}{d\omega_\gamma d\Omega_\pi d\Omega_\gamma} &= \frac{(2\pi)^4 \omega_\gamma m_N^2}{8|\vec{q} E(\vec{p}) - \vec{p} \omega(\vec{q})|} \int \frac{d|\vec{q}'| |\vec{q}'|^2}{(2\pi)^3 \omega(\vec{q}')} \int \frac{d\vec{p}'}{(2\pi)^3 E(\vec{p}')} \delta^4(p + q - p' - q' - k) \\ &\times \frac{1}{2} \sum_{\epsilon_\lambda, ms', ms} \left| \mathcal{M}[\pi^+p \rightarrow \pi^+p\gamma](\epsilon_\lambda, k; q', p', ms'; q, p, ms) \right|^2, \end{aligned} \quad (7)$$

where $k = (\omega_\gamma, \vec{k})$ and ϵ_λ are the four-momentum and polarization four-vector of the photon, respectively. In section 4.2, we will compare this cross section calculated in our model with

a set of experimental data⁵ in order to extract a value for the magnetic dipole moment of the Δ^{++} baryon resonance.

The amplitude for radiative π^+p scattering can be obtained by attaching the photon to all external and internal lines in Feynman diagrams of elastic scattering (shown in Figure 1). In addition, we will also have four-point vertices involving the photon (see Figure 2). Such vertices arise from the derivative couplings of baryons and mesons in Eqs. (3). The Feynman rules required to introduce electromagnetism are derived from the following effective Lagrangian:

$$\hat{\mathcal{L}}_{elec} = \hat{\mathcal{L}}_{\gamma NN} + \hat{\mathcal{L}}_{\gamma\pi NN} + \hat{\mathcal{L}}_{\gamma\pi\pi} + \hat{\mathcal{L}}_{\gamma\Delta\Delta} + \hat{\mathcal{L}}_{\gamma\pi N\Delta} + \hat{\mathcal{L}}_{\gamma\rho\pi\pi} + \hat{\mathcal{L}}_{\gamma\sigma\pi\pi}. \quad (8)$$

The different pieces of this Lagrangian are the following:

$$\begin{aligned} \hat{\mathcal{L}}_{\gamma NN}(x) &= -e\bar{\psi}(x) \left[\gamma_\mu - \frac{\kappa_p}{2m_N} \sigma_{\mu\nu} \partial^\nu \right] A^\mu(x) \psi(x), \\ \hat{\mathcal{L}}_{\gamma\pi NN}(x) &= -e \left(\frac{f_{\pi NN}}{m_\pi} \right) \bar{\psi}(x) \gamma_5 \gamma_\mu [\vec{\tau} \times \vec{\pi}(x)]_3 \psi(x) A^\mu(x), \\ \hat{\mathcal{L}}_{\gamma\pi\pi}(x) &= -e [\vec{\pi}(x) \times \partial_\mu \vec{\pi}(x)]_3 A^\mu(x), \\ \hat{\mathcal{L}}_{\gamma\Delta\Delta}(x) &= -2e\bar{\psi}_{\Delta\nu}(x) \Lambda^{\nu\nu'}(A) \Gamma_{\nu'\mu'\alpha} \Lambda^{\mu'\mu}(A) \psi_{\Delta\mu}(x) A^\alpha(x), \\ \hat{\mathcal{L}}_{\gamma\Delta\pi N}(x) &= e \left(\frac{f_{\Delta\pi N}}{m_\pi} \right) \bar{\psi}_\Delta^\mu(x) \Lambda_{\mu\nu}(A) [\vec{\pi}(x) \times \vec{T}^\dagger]_3 \psi(x) A^\nu(x) + h.c., \\ \hat{\mathcal{L}}_{\gamma\rho\pi\pi}(x) &= eg_\rho \{ [\vec{\pi}(x) \cdot \vec{\pi}(x) - \pi_3(x)\pi_3(x)] \rho_3^\nu(x) \\ &\quad - \pi_3(x) [\vec{\pi}(x) \cdot \vec{\rho}^\nu(x) - \pi_3(x)\rho_3^\nu(x)] \} A_\nu(x), \\ \hat{\mathcal{L}}_{\gamma\sigma\pi\pi}(x) &= -2e \left(\frac{g_{\sigma\pi\pi}}{2m_\pi} \right) \sigma(x) [\vec{\pi}(x) \times \partial_\mu \vec{\pi}(x)]_3 A^\mu(x), \end{aligned} \quad (9)$$

where $A_\nu(x)$ is the electromagnetic four-potential and e (κ_p) denotes the charge (anomalous magnetic moment) of the proton. The tensor $\Lambda_{\mu\nu}(A)$ has been defined in the previous section. The interaction Lagrangians of Eq. (9) involving the Δ are invariant under the contact transformations of Eq. (4).

The electromagnetic vertex of the Δ^{++} resonance is given by [11, 15]:

$$\Gamma_{\alpha\beta\rho} = \left(\gamma_\rho - \frac{i\kappa_\Delta}{2m_\Delta} \sigma_{\rho\sigma} k^\sigma \right) g_{\alpha\beta} - \frac{1}{3} \gamma_\rho \gamma_\alpha \gamma_\beta - \frac{1}{3} \gamma_\alpha g_{\beta\rho} + \frac{1}{3} \gamma_\beta g_{\alpha\rho}, \quad (10)$$

where we have allowed for a term describing the anomalous magnetic moment κ_Δ of the Δ resonance. This quantity is related to the total magnetic dipole moment of the Δ^{++} through

⁵ In particular, this observable will be represented as a function of the photon energy ω_γ for fixed angular configurations of photons and pions emitted in the process.

the following equation:

$$\mu_\Delta = 2(1 + \kappa_\Delta) \frac{e}{2m_\Delta}. \quad (11)$$

It is straightforward to verify that the vertex of Eq. (10) satisfies the following Ward identity:

$$G^{\mu\alpha}(P') \Gamma_{\alpha\beta\rho} k^\rho G^{\beta\nu}(P) = G^{\mu\nu}(P) - G^{\mu\nu}(P') \quad (12)$$

where $P = P' + k$. This identity (together with the inclusion of *all* possible radiative diagrams) guarantees that the radiative $\pi^+ p$ scattering amplitude computed with the Feynman rules of Eqs. (3) and (9) is automatically gauge-invariant, even when the complex mass scheme is implemented.

The interaction Lagrangians shown in Eqs. (3) and (9) give rise to the Feynman diagrams displayed in Figure 2. The first line of Fig. 2 contains the contributions with the Δ^{++} as intermediate state. The other two lines in Figure 2 correspond to the contributions with intermediate Δ^0 , N and $\rho - \sigma$ mesons. The evaluation of these gauge-invariant contributions is straightforward. Therefore, as in the case of elastic scattering, we will focus on the amplitude corresponding to the Δ^{++} exchange in the s -channel. This amplitude receives contributions from the seven Feynman graphs appearing in the first row of Figure 2; it is given by [15]:

$$\begin{aligned} \mathcal{M}_{\Delta^{++}}(\pi^+ p \rightarrow \pi^+ p \gamma) &= -ie \left(\frac{f_{\Delta\pi N}}{m_\pi} \right)^2 q'_\mu q_\nu \bar{u}(p') \left[G^{\mu\nu}(P') \left(\frac{q \cdot \epsilon}{q \cdot k} + \frac{p \cdot \epsilon - R(p) \cdot \epsilon}{p \cdot k} \right) \right. \\ &\quad - \left(\frac{q' \cdot \epsilon}{q' \cdot k} + \frac{p' \cdot \epsilon - R(p') \cdot \epsilon}{p' \cdot k} \right) G^{\mu\nu}(P) + 2G^{\mu\alpha}(P') \Gamma_{\alpha\beta\rho} \epsilon^\rho G^{\beta\nu}(P) \\ &\quad \left. + \frac{1}{q \cdot k} G^{\mu\rho}(P') (\epsilon_\rho k^\nu - \epsilon^\nu k_\rho) - \frac{1}{q' \cdot k} (\epsilon^\mu k_\rho - \epsilon_\rho k^\mu) G^{\rho\nu}(P) \right] u(p) \quad (13) \end{aligned}$$

where

$$R_\mu(x) \equiv \frac{1}{4} [\not{k}, \gamma_\mu] + \frac{\kappa_p}{8m_N} \{[\not{k}, \gamma_\mu], \not{x}\},$$

and $P = p + q$, $P' = p' + q'$, such that $P = P' + k$. This amplitude exhibits the correct low photon energy behavior expected by Low's theorem [14].

As required, this amplitude is explicitly gauge-invariant (*i.e.*, it vanishes when $\epsilon \rightarrow k$ by virtue of the Ward identity given in Eq. (12)) and does not depend on the parameter A associated to contact transformations. As it was discussed in the previous section, finite width effects of the Δ^{++} are necessary in order to avoid that the amplitude diverges when

P^2 or P'^2 approaches m_Δ^2 . According to the prescription of the complex mass scheme, we can perform the replacement $m_\Delta^2 \rightarrow m_\Delta^2 - im_\Delta\Gamma_\Delta$ in the propagator and the electromagnetic vertex of the Δ^{++} without destroying gauge-invariance.

4. Comparison with experimental data

In this section we compare our dynamical model with experimental data on elastic and radiative π^+p scattering. We are not interested in performing a global fit to the whole universe of experimental data about these processes. Our first goal in section 4.1 is to test how our model works in the case of elastic π^+p scattering. By using a reliable set of experimental data on the total cross section for this process, we fix the free parameters of our model: the mass and width of the Δ and its coupling to π^+p . With this information at hand, we will compare the *prediction* of our model with available experimental data on the differential cross section of elastic π^+p scattering. Finally, in section 4.2 we use a set of experimental data on radiative π^+p scattering to extract the value of the magnetic dipole moment of the Δ^{++} , which is left as the only free parameter of the model in this case.

4.1 Elastic π^+p scattering: fixing the mass and width of the Δ

The different contributions to the elastic π^+p scattering amplitude are shown in Fig.1. The amplitude corresponding to the Δ^{++} resonance in the s -channel was given explicitly in Eqs. (5) and (6). This is the most important contribution to elastic scattering in the resonance region ($T_{lab} \approx 175$ MeV). All other contributions should be added coherently, and the total amplitude $\mathcal{M}[\pi^+p \rightarrow \pi^+p]$ exhibits the resonant plus background structure expected by general principles of S -matrix theory [13]. Finally we use Eq.(1) to evaluate the total elastic cross section.

Some of the couplings that enter the interaction Lagrangians given in Eq.(3) are taken from other low energy processes. For example, the coupling constants $(g_\rho^2, g_{\pi NN}^2)/4\pi = (2.9, 14)$ were taken from the $\rho\pi\pi$ decays and the analysis of NN scattering data [12, 24], whereas the magnetic ρNN coupling $\kappa_\rho = 3.7$ was extracted from values of nucleon magnetic moments. The masses of the ρ meson and the nucleon were taken from [1], and the mass of the hypothetical σ meson was set to 650 MeV [12, 24] (see the end of this section for other choices of this mass). Thus, the mass and width of the Δ and the coupling constants

$g_{\sigma\pi\pi, \sigma NN}$ and $f_{\Delta N\pi}$ are left as the only free parameters to be determined from the total cross section of π^+p scattering.

In order to compare the size of the different contributions, we have fitted the total cross section by adding successively, a new background contribution (diagrams with Δ^0 , N , ρ and σ in intermediate states) in each fit. The results of these fits are shown in Table 1. The curves corresponding to every one of the best fits to the experimental cross sections of Ref. [25] are plotted in Figure 3, for energies of incident pions in the range $75 \text{ MeV} \leq T_{lab} \leq 300 \text{ MeV}$.

Once we have fitted the free parameters relevant for elastic π^+p scattering, we can give an additional non-trivial check of the model. This corresponds to the prediction of the differential cross section $d\sigma/d\Omega_\pi$ as a function of the scattering pion angles θ , for fixed energies of incident pions. In Figure 4, we have compared our predictions for the differential cross section with some available experimental data [26, 27, 28] for $T_{lab} \approx 263$ and 291 MeV, in a wide interval of scattering angles.

Some interesting features are worth to be stressed from the fits to the total and differential cross sections of elastic π^+p scattering. First, we can observe that agreement with data in both cases is improved when the contributions from all intermediate states (Δ^{++} , Δ^0 , N , ρ and σ) are included. The values of χ^2/dof are reasonably good given the uncertainties inherent to the model⁶(mainly related to the uncertainty in the mass σ meson meson). In particular, the contribution from the σ meson allows to achieve a better fit to the total cross section for T_{lab} below the resonance peak (see Fig. 3). It also allows to improve the agreement with the differential cross section (see Figure 4) in the whole angular interval considered here. Second, the values obtained for the mass and width of the Δ 's, namely $m_\Delta = (1211.2 \pm 0.4)$ MeV and $\Gamma_\Delta = (88.2 \pm 0.4)$ MeV, are similar to those obtained from a model-independent analysis of the same data on the total cross section, namely [21]: $M = (1212.20 \pm 0.23)$ MeV and $\Gamma = (97.06 \pm 0.35)$ MeV⁷. This comparison provides a consistency check for our model as long as both results corresponds to the mass and width parameters defined from the pole position of the scattering amplitude. Note, however, that this agreement is non trivial because in our model the background contributions are *fixed* from independent low-energy phenomenology. This is not the case within the S -matrix approach to the π^+p amplitude [21], where the background terms are taken as slowly varying functions to be fitted to experimental

⁶ The $\chi^2/d.o.f.$ obtained in the last fit involving all the contributions, drops to 4.5 when the last three points in the upper tail of the total cross section are excluded.

⁷As is well known, the parameters defined from the pole position are smaller than the ones obtained using a Breit-Wigner formula with energy-dependent width [1].

data. In other words, contributions to the elastic amplitude with Δ^0 , N , ρ and σ , indeed simulate well the background terms obtained from the model-independent analysis of Ref. [21].

It is interesting to observe in Figure 4 that the model describes well the differential cross section despite the fact that these data correspond to kinetic energies of incident pions ($T_{lab} \approx 263$ and 291 MeV) that lie at the upper tail of the Δ^{++} resonance shape (see Figure 3). This is very important because incident pions in radiative π^+p scattering, to be considered below, correspond to those particular values of kinetic energies.

Finally one may wonder how the particular value of the σ meson mass ($m_\sigma = 650$ MeV) could have influenced the fitting procedure. We have repeated the fits to the total cross section data by allowing m_σ to vary 200 MeV around its central value. The results are shown in Table 2 and Figure 5 for the total cross section. Figure 6 shows the corresponding predictions for the differential cross section. From Table 2 and Figure 5, we observe that the mass of the σ meson is mainly correlated with its coupling constants to pions and nucleons, while the changes in the Δ parameters are negligible. On the other hand, the effects of these variations in the mass of the σ meson can be more important in the differential cross section of elastic π^+p scattering. Note however that our prediction for this observable becomes worse for $\cos\theta > 0$ when m_σ deviates from 650 MeV (see Figure 6), although it may slightly improve the prediction for negative values of $\cos\theta$. Consequently, in the following we will take $m_\sigma = 650$ MeV in our fitting procedure.

4.2 Radiative π^+p scattering: determination of μ_Δ

The contributions to the radiative π^+p scattering amplitude are shown in Figure 2. The scattering amplitudes corresponding to the last two rows in Fig. 2 can be computed in a straightforward way. The amplitudes involving the Δ^{++} resonance, first row in Figure 2, have to take into account the finite width effect of this resonance, preserve gauge invariance and remain invariant under contact transformations. This amplitude has been given explicitly in Eq. (13).

Based on the analysis presented in the previous section, we can easily check that the only free parameter in our description of radiative π^+p scattering is the Δ^{++} magnetic dipole moment. Thus, a fit to the corresponding radiative data should provide us with a determination of this important property.

In order to justify our choice of experimental data, let us remember the structure of photon radiation in π^+p scattering. As is well known [14], the low photon-energy structure of the unpolarized probability of radiative processes is given by:

$$\sum_{\epsilon_\lambda} |\mathcal{M}(\pi^+p \rightarrow \pi^+p\gamma)|^2 = \frac{A}{\omega_\gamma^2} + B\omega_\gamma^0 + \dots \quad (14)$$

The terms of $O(\omega_\gamma^{-2})$ arise from photons radiated off external charged particles and A depends only on the parameters of elastic π^+p scattering. Terms of order ω_γ^{-1} are absent in the unpolarized probability by virtue of the Burnett and Kroll's theorem [29]. The effects of the Δ^{++} magnetic dipole moment enter this probability at order ω_γ^0 . Thus, for low-energy photons, we expect the unpolarized probability to be sensitive to the effects of the Δ^{++} MDM when some kinematical mechanisms allows to suppress the leading dominant term (of $O(\omega_\gamma^{-2})$). Fortunately, this situation occurs when photons are emitted in a backward configuration to other charged particles [30]. Actually, this has been the motivation to study those particular geometrical configurations of radiative π^+p scattering in Ref. [8].

Thus, the experimental data of Ref. [8] are suitable for a determination of the Δ^{++} magnetic dipole moment within our model. Furthermore, since we expect our approximation to be more reliable for low-energy photons (where the electromagnetic static properties play the main role), we will chose a subset of data corresponding to $20 \text{ MeV} \leq \omega_\gamma \leq 100 \text{ MeV}$. Following Ref. [8] we label with G1, G4 and G7 the geometrical configurations corresponding to photons detected at angles $(\theta_\gamma, \phi_\gamma) = (160^\circ, 0^\circ)$, $(140^\circ, 0^\circ)$ and $(120^\circ, 0^\circ)$, respectively; *i.e.* the photons emitted backwards to the outgoing pion, which in turn is emitted at angle $(\theta_\pi, \phi_\pi) = (50.5^\circ, 180^\circ)$ with respect to the direction of incident pions. As already explained, we expect these configurations to be more sensitive to the effect of the Δ^{++} MDM⁸. Once we would have obtained a value of μ_Δ from those configurations, we would compare the results of our model with experimental data for other geometrical configurations of photons.

The fits of our model to the experimental data of Ref. [8] yield the determinations of the magnetic dipole moment shown in Table 3, for the three photon geometries and for two different energies of incident pions: $T_{lab} = 269$ and 298 MeV . The fitted curves to $d\sigma/d\omega_\gamma d\Omega_\pi d\Omega_\gamma$ (Eq.(7)) are represented with solid lines in Figures 7 (for $T_{lab} = 269 \text{ MeV}$) and 8 (for $T_{lab} = 298 \text{ MeV}$). In Figure 7 we have also included the curve (dashed line)

⁸One may also chose to fit the whole set of UCLA data to quote an average value for the MDM (see for example Ref. [5]). However, it is reasonable to expect that the set of data that is most sensitive to the effects of the MDM probes the underlying dynamics in a more detailed way.

corresponding to $\kappa_\Delta = 1$, in order to visualize the sensitivity of the differential cross section to the Δ^{++} MDM for those particular geometrical configurations. Although the experimental data are rather scarce, Fig. 7 clearly indicates that the photon spectrum for the G1, G4 and G7 geometries is indeed sensitive to the effect of the Δ^{++} MDM.

In order to compare the sensitivity of different photon configurations, we have displayed in Figure 9 the best fit for the G7 configuration ($\kappa_\Delta = 3.27 \pm 0.76$) together with the cross section evaluated at the same value of κ_Δ for the configurations G11=(160°, 180°) and G14=(103°, 180°), for incident pions of energy $T_{lab} = 269$ MeV⁹. We observe that the curve corresponding to $\kappa_\Delta = 1$ (dashed line) is indistinguishable from the ones corresponding to value $\kappa_\Delta = 3.27$ (full line), for the G11 and G14 geometries.

The different determinations of κ_Δ shown in Table 3 are consistent among themselves. Therefore, we consider meaningful to quote a weighted average over the six different fits. If we express the weighted average in units of nuclear magnetons we obtain:

$$\mu_\Delta = 2(1 + \kappa_\Delta) \frac{m_p}{m_\Delta} \left(\frac{e}{2m_p} \right) = (6.14 \pm 0.51) \frac{e}{2m_p}. \quad (15)$$

Our result in Eq. (15) is compared in Table 4 with some of the experimental determinations and theoretical calculations of the Δ^{++} magnetic dipole moment that are available in the literature. Eq. (15) is compatible with the prediction $\mu_\Delta = 5.58(e/2m_p)$ obtained in the SU(6) spin-flavor symmetry of the quark model [31] and with the result obtained from the QCD and pion corrections in the chiral bag-model [32]; however our result is somewhat larger than the prediction obtained from the bag-model corrections to the SU(6) quark model, $\mu_\Delta = (4.41 \sim 4.89)(e/2m_p)$ [34]. Eq. (15) is consistent with some previous determinations of the MDM, for example with: $\mu_\Delta = (5.6 \sim 7.5)(e/2m_p)$ from Ref. [4], $(5.6 \pm 2.1)(e/2m_p)$ from Ref. [6] and $(6.9 \sim 9.8)(e/2m_p)$ from [3]. However, the central value in Eq. (15) disagrees with some other available determinations, namely: $\mu_\Delta = (3.6 \pm 2)(e/2m_p)$ from [2] obtained by using a relativistic model, and the result of Ref. [5], $(3.7 \sim 4.9)(e/2m_p)$, which is obtained using a soft-photon approximation.

Using the average value of μ_Δ quoted in Eq. (15), we can compare the results of our model with other angular configurations of photon emission (labeled G1-G19 in Ref. [8]). The χ^2 values obtained by comparing our prediction for $d\sigma/d\omega_\gamma d\Omega_\pi d\Omega_\gamma$ and the corresponding experimental values for the 18 detection angles, are shown in Tables 5 and 6, respectively,

⁹It is important to stress that a direct fit for these configurations is not significant due to the small sensitivity of this observable upon κ_Δ

for incident pions energies $T_{lab} = 269$ MeV and $T_{lab} = 298$ MeV. For illustrative purposes, in Figures 10 and 11 we have compared the theoretical prediction based on Eq. (15) to experimental data of Ref. [8] for the special configurations G10-G15. According to the χ^2 values shown in Tables 5 and 6, we can conclude that our model satisfactorily describes a large set of data of Ref. [8].

5. Conclusions

In the present paper we have used electromagnetic gauge invariance and invariance under contact transformations as guiding principles to provide a determination of the Δ^{++} magnetic dipole moment within a full dynamical model for the low energy interactions of this resonance. Our description of elastic and radiative π^+p scattering consistently incorporate the finite width effects of the Δ^{++} . The interaction vertices involving this resonance do not require the inclusion of *ad hoc* form factors: vertices correspond to structureless interactions as expected in the low energy regime. Resonant and background contributions to the elastic and radiative π^+p scattering amplitudes are cleanly separated, as demanded by general principles of S -matrix theory.

The relevant parameters of the Δ^{++} resonance (other than the magnetic dipole moment) are fixed from the total cross section of elastic π^+p scattering. The values obtained for the mass and width of the Δ^{++} are very close to the ones obtained for these pole parameters in a model-independent analysis of the π^+p total cross section based on the S -matrix theory [21]. The prediction for the differential cross section of elastic scattering is found to be in very good agreement with available experimental data. This consistency check assures that our dynamical model gives a good description of background contributions to elastic scattering as provided by the Δ^0 , N , ρ and σ intermediate states.

The magnetic dipole moment of the Δ^{++} turns out to be the only adjustable parameter in radiative π^+p scattering. Using the most sensitive configurations of emitted photons, we have fitted the available data of $d\sigma/d\omega_\gamma d\Omega_\pi d\Omega_\gamma$ in the low-energy photon regime. We have found:

$$\mu_\Delta = (6.14 \pm 0.51) \frac{e}{2m_p} .$$

Our result is consistent with predictions based on the simplest version of SU(6) the quark model [31].

With the value (Eq. (15)) extracted from the most sensitive angular configurations in radiative π^+p scattering, we can reproduce very well a wider set of experimental data of Ref. [8]. This conclusion is based in the low χ^2/dof values given in Tables 5 and 6, and the illustrative plots shown in Figures 10 and 11.

Acknowledgements: The work of A. M. was supported by Conacyt (México). G.L.C. acknowledges partial support from Conacyt, under contract 32429-E.

References

- [1] D. E. Groom *et al*, Particle Data Group, Eur. Phys. J. **C15**, 1 (2000).
- [2] M. M. Musakhanov, Sov. J. Nuc. Phys. **19**, 319 (1974).
- [3] L. Heller, S. Kumano, J.C. Martinez and E. J. Moniz, Phys. Rev. **C35**, 718 (1987)
- [4] R. Wittman, Phys. Rev. **C37**, 2075 (1988).
- [5] D. Lin , M.K. Liou and Z.M. Ding, Phys. Rev. **C44**, 1819 (1991).
- [6] P. Pascual and R. Tarrach, Nucl. Phys. **B134**, 133 (1978).
- [7] A. Bosshard *et al*, Phys. Rev. **D44**, 1962 (1991) ; C. A. Meyer et al., Phys. Rev. **D38**, 754 (1988).
- [8] B. M. K. Nefkens *et al*, Phys. Rev. **D18**, 3911 (1978).
- [9] M. Arman *et al*, Phys. Rev. Lett. **29**, 962 (1972).
- [10] K. C. Leung *et al*, Phys. Rev. **D14**, 698 (1976).
- [11] L. M. Nath, B. Etemadi, and J. D. Kimel, Phys. Rev. **D3**, 2153 (1971); R. E. Behrends and C. Fronsdal, Phys. Rev. **106**, 277 (1958); J. Urías, Ph. D. Thesis, Université Catholique de Louvain, Belgium (1976).
- [12] C. Schütz, J.W. Durso, K. Holinde, and J. Speth, Phys. Rev. **C49**, 2671(1994).
- [13] R. E. Peierls, *Proc. of the 1954 Glasgow Conf. on Nucl. and Meson Physics*, Ed. E. H. Bellamy and R. G. Moorhouse (Pergamon Press, 1955), p. 296; R. Eden, P. Landshoff, D. Olive, and J. Polkinghorne, “The Analytic S-matrix” (Cambridge University Press, Cambridge, 1966); M. Lévy, Nuovo Cim. **13**, 115 (1959).

- [14] F. E. Low, Phys. Rev. **110**, 974 (1958).
- [15] M. El-Amiri, G. López Castro and J. Pestieau, Nucl. Phys. **A543**, 673 (1992).
- [16] G. López Castro and A. Mariano, e-print nucl-th/0006037.
- [17] R. G. Stuart, Phys. Lett. **B262**, 113 (1991); **272**, 353 (1991); Phys. Rev. Lett. **70**, 3193 (1993); A. Sirlin, Phys. Rev. Lett. **67**, 2127 (1991); H. Veltman, Z. Phys. **C62**, 35 (1994).
- [18] U. Baur and D. Zeppenfeld, Phys. Rev. Lett. **75**, 1002 (1995); E. Argyres *et al*, Phys. Lett. **B358**, 339 (1995); M. Beuthe *et al* Nucl. Phys. **B498**, 55 (1997); W. Beenakker *et al*, Nucl. Phys. **B500**, 255 (1997).
- [19] G. López Castro and G. Toledo Sánchez, Phys. Rev. **D61**, 033007 (2000).
- [20] A. Mariano and G. López Castro, Phys. Rev. **62**, 014604(2000).
- [21] A. Bernicha, G. López Castro and J. Pestieau, Nucl. Phys. **A597**, 623 (1996).
- [22] G. López Castro, J. L. Lucio M., and J. Pestieau, Mod. Phys. Lett. **A**, (1991); Int. J. Mod. Phys. **A10**, (1996).
- [23] A. Pilaftsis and M. Nowakowski, Z. Phys. **C60**, 121 (1993).
- [24] See for example: B.C. Pearce and B.K. Jennings, Nucl. Phys.,**A528**,655 (1991); C. Lee, S.N. Yang, and T.-S.H. Lee, J. Phys. **G17**, L131 (1991).
- [25] E. Pedroni *et al*, Nucl. Phys. **A300**, 321(1978).
- [26] P.J. Bussey *et al*, Nuc. Phys. **B58**, 363(1973).
- [27] M.E. Sadler *et al*, Phys. Rev. **D35**, 2718 (1987).
- [28] V.A. Gordeev *et al*, Nuc. Phys. **A364**, 408 (1981).
- [29] T. H. Burnett and N. M. Kroll, Phys. Rev. Lett. **20**, 86 (1968).
- [30] V. I. Zakharov, L. A. Kondratyuk, and L. A. Ponomarev, Yad. Fiz. **8**, 783 (1968) [Sov. J. Nucl. Phys. **8**, 456 (1968)].
- [31] M. A. B. Beg, B. W. Lee and A. Pais, Phys. Rev. Lett. **13**, 514 (1964).

- [32] M. I. Krivoruchenko, *Sov. Jour. Nucl. Phys.* **45**, 109 (1987).
- [33] M. A. B. Beg and A. Pais, *Phys. Rev.* **137**, B1514 (1965)
- [34] G. E. Brown, M. Rho and V. Vento, *Phys. Lett.* **B97**, 423 (1980).

TABLE CAPTIONS

Table 1: Yields from the fits to the total cross section of the elastic π^+p scattering by including the different intermediate states ($g_\sigma \equiv g_{\sigma\pi\pi}g_{\sigma NN}$).

Table 2: Fits to the cross section of the elastic π^+p scattering including $\Delta^{++}, N, \rho,$ and σ degrees of freedom for different values of m_σ .

Table 3: Fits to the differential cross section of radiative π^+p scattering, for three different geometries of photon angle emission and two different energies of incident pions.

Table 4: Some of the experimental determinations and theoretical calculations of the Δ^{++} magnetic dipole moment.

Table 5: $\chi^2/(\# \text{ data})$ values obtained from the comparison between our model (based on Eq. (15)) and experimental data, for the differential cross section of radiative π^+p scattering at $T_{lab}=269$ MeV. G1-G19 label the geometrical configurations as in Ref. [8].

Table 6: Same as Table 5 for $T_{lab}=298$ MeV.

FIGURE CAPTIONS

Figure 1: Feynman graphs corresponding to the different contributions to the elastic π^+p scattering amplitude.

Figure 2: Feynman graphs for the radiative π^+p amplitude: s -, crossed-, and t -channels correspond to Δ^{++} , (Δ^0, N) and (ρ, σ) contributions in intermediate states, respectively.

Figure 3: Total cross section of elastic π^+p scattering as a function of incident π^+ kinetic energy.

Figure 4: Differential cross section of elastic π^+p scattering. Circles, triangles and squares denote, respectively, experimental data from Refs.[26, 27, 28]. The curves (with same convention as in Figure 1) denote our prediction for $T_{lab} = 263.7$ MeV (upper box) and $T_{lab} = 291.4$ MeV (lower box).

Figure 5: Elastic π^+p total cross section as a function of incident π^+ kinetic energy obtained for three different masses of the σ meson.

Figure 6: Differential cross section of elastic π^+p scattering, for $T_{lab} = 263.7$ MeV (upper box) and $T_{lab} = 291.4$ MeV (lower box) and $m_\sigma = 450, 650$ and 850 MeV. Line conventions are those of Figure 5 and experimental results correspond to Refs.[26, 27, 28].

Figure 7: Differential cross section of radiative π^+p scattering for $T_{lab} = 269$ MeV. The G1, G4 and G7 geometries are defined in Table 2. The solid line corresponds to the best fit and the dashed line to $\kappa_\Delta = 1$.

Figure 8: Same as in Figure 7 when $T_{lab} = 298$ MeV.

Figure 9: Same as in Figure 7 for the G7, G11, and G14 configurations, but the full lines correspond in all cases to values of κ_Δ obtained from the best fitting for G7 case (see section 4.2).

Figure 10: Differential cross section of radiative π^+p scattering for $T_{lab} = 269$ MeV and the G10-G15 configurations [8]. The solid lines correspond to the prediction based on Eq. (15).

Figure 11: Same as in Figure 10 when $T_{lab} = 298$ MeV [8].

Interm. state	$f_{\Delta N\pi}^2/4\pi$	m_{Δ} (MeV)	Γ_{Δ} (MeV)	$g_{\sigma}/4\pi$	χ^2/dof
$\Delta^{++,0}$	0.281 ± 0.001	1201.7 ± 0.2	69.8 ± 0.2	–	121.1
$\Delta^{++,0}, N$	0.331 ± 0.003	1208.6 ± 0.2	87.5 ± 0.3	–	17.6
$\Delta^{++,0}, N, \rho$	0.327 ± 0.001	1207.4 ± 0.2	85.6 ± 0.3	–	15.6
$\Delta^{++,0}, N, \rho, \sigma$	0.317 ± 0.003	1211.2 ± 0.4	88.2 ± 0.4	1.50 ± 0.12	10.5

Table 1

m_{σ} [MeV]	$f_{\Delta N\pi}^2/4\pi$	m_{Δ} (MeV)	Γ_{Δ} (MeV)	$g_{\sigma\pi\pi}g_{\sigma NN}/4\pi$
450	0.311 ± 0.002	1211.3 ± 0.3	86.4 ± 0.3	1.00 ± 0.05
650	0.317 ± 0.003	1211.2 ± 0.4	88.2 ± 0.4	1.50 ± 0.11
850	0.318 ± 0.003	1211.1 ± 0.4	88.5 ± 0.4	1.90 ± 0.18

Table 2

T_{lab} (MeV)	Geometry	θ_{γ}	ϕ_{γ}	κ_{Δ}	χ^2/dof
269	G7	120^0	0^0	3.27 ± 0.76	1.99
	G4	140^0	0^0	3.01 ± 0.67	2.48
	G1	160^0	0^0	2.74 ± 0.87	1.73
298	G7	120^0	0^0	3.10 ± 0.87	2.68
	G4	140^0	0^0	2.90 ± 0.75	4.75
	G1	160^0	0^0	2.61 ± 1.00	1.47

Table 3

Source	$\mu_{\Delta} \times e/2m_p$	Experimental data	Method/model
	Experimental determinations		
Ref. [2]	3.6 ± 2.0	Ref. [9]	Relativistic
Ref. [6]	5.64 ± 2.13	Ref. [10]	Relativistic
Ref. [8]	$4.7 \sim 6.7$	Ref. [8]	Model of Ref. [6] and Soft-photon approx. (SPA)
Ref. [3]	$6.9 \sim 9.8$	Ref. [8]	MIT isobar of Ref. [3]
Ref. [4]	$5.6 \sim 7.5$	Ref. [8]	Relativistic
Ref. [7]	4.58 ± 0.33	Ref. [7]	MIT isobar [3]
Ref. [5]	$3.7 \sim 4.9$	Ref. [8, 7]	Modified SPA
Present work	6.14 ± 0.51	Ref. [8]	Relativistic
	Theoretical calculations		
Ref. [31]	5.58	–	SU(6) symmetry
Ref. [33]	4.25	–	Mass corrections to SU(6)
Ref. [34]	$4.41 \sim 4.89$	–	π -cloud corr. to SU(6)
Ref. [32]	6.54	–	QCD corr. in χ bag-model

Table 4

T_{lab} (MeV)	Geometry	θ_γ	ϕ_γ	$\chi^2/(\# \text{ data})$
269	G1	160 ⁰	0 ⁰	0.8
	G2	153.3 ⁰	316.5 ⁰	2.1
	G3	139.5 ⁰	295.2 ⁰	2.6
	G4	160 ⁰	0 ⁰	2.
	G5	136 ⁰	333.2 ⁰	1.7
	G6	128.3 ⁰	311.5 ⁰	8.7
	G7	120 ⁰	0 ⁰	2.1
	G8	118.4 ⁰	339.4 ⁰	6.1
	G9	113.8 ⁰	320 ⁰	3.7
	G10	144 ⁰	270 ⁰	0.5
	G11	160 ⁰	180 ⁰	2.3
	G12	140 ⁰	180 ⁰	1.5
	G13	120 ⁰	180 ⁰	0.7
	G14	103 ⁰	180 ⁰	0.9
	G15	102.2 ⁰	200.5 ⁰	0.40
	G17	50.1 ⁰	174.8 ⁰	1.
	G18	64.6 ⁰	293.4 ⁰	0.8
	G19	59 ⁰	270 ⁰	0.3

Table 5

T_{lab} (MeV)	Geometry	θ_γ	ϕ_γ	$\chi^2/(\# \text{ data})$
298	G1	160 ⁰	0 ⁰	0.4
	G2	153.3 ⁰	316.5 ⁰	0.2
	G3	139.5 ⁰	295.2 ⁰	0.9
	G4	160 ⁰	0 ⁰	3.6
	G5	136 ⁰	333.2 ⁰	2.8
	G6	128.3 ⁰	311.5 ⁰	0.6
	G7	120 ⁰	0 ⁰	2.4
	G8	118.4 ⁰	339.4 ⁰	0.5
	G9	113.8 ⁰	320 ⁰	2.7
	G10	144 ⁰	270 ⁰	1.
	G11	160 ⁰	180 ⁰	0.4
	G12	140 ⁰	180 ⁰	4.9
	G13	120 ⁰	180 ⁰	2.4
	G14	103 ⁰	180 ⁰	1.
	G15	102.2 ⁰	200.5 ⁰	0.5
	G17	50.1 ⁰	174.8 ⁰	0.8
	G18	64.6 ⁰	293.4 ⁰	1.1
	G19	59 ⁰	270 ⁰	1.31

Table 6

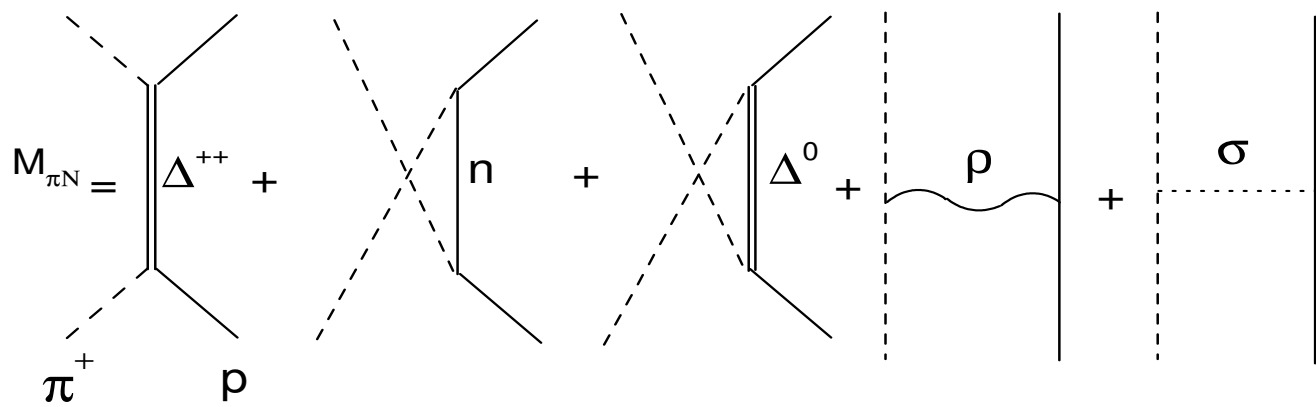


Figure 1

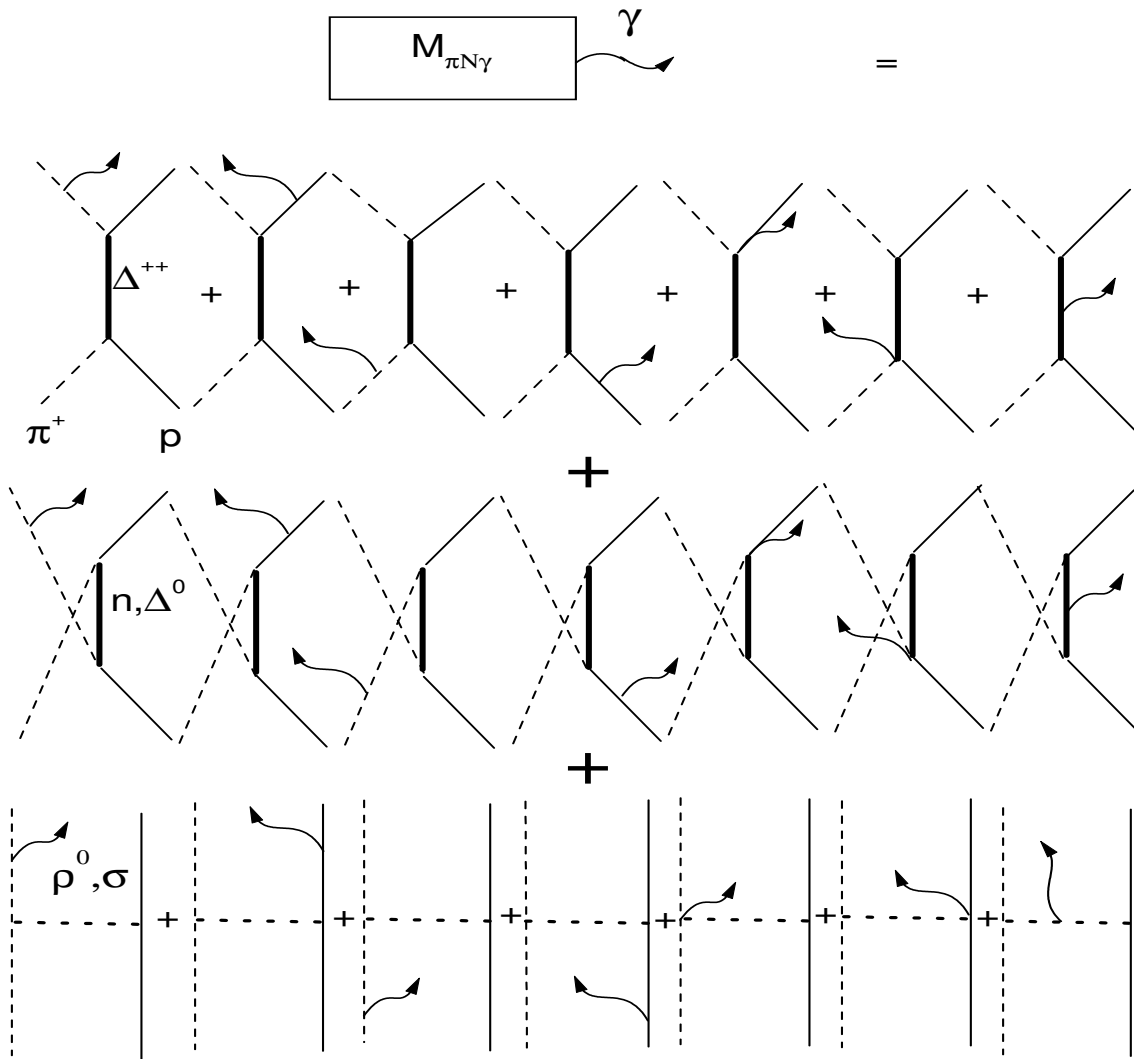


Figure 2

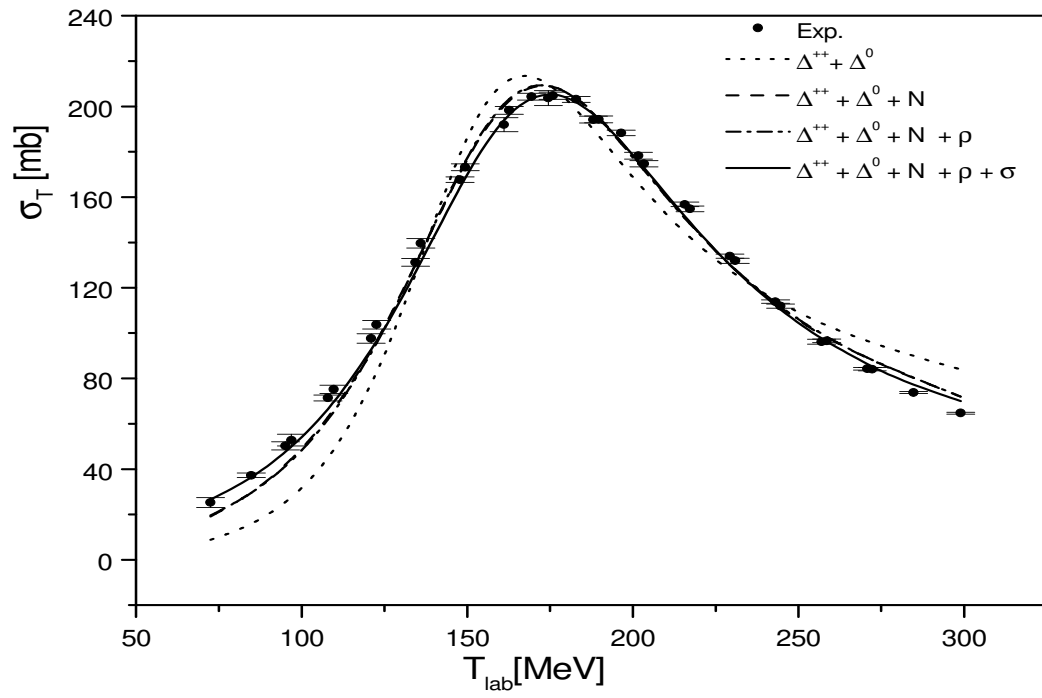


Figure 3

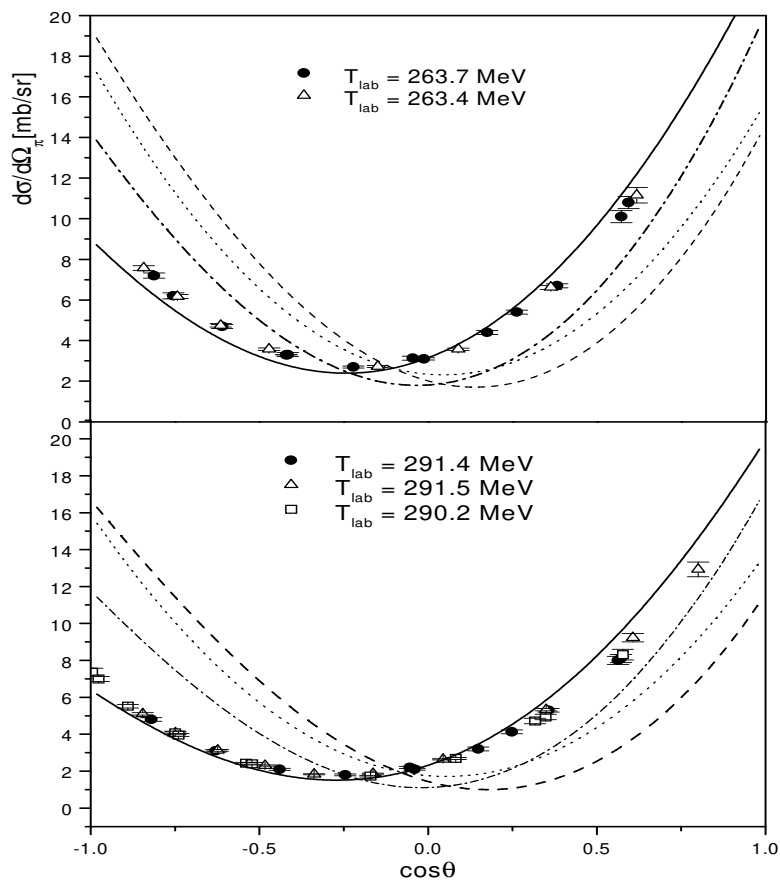


Figure 4

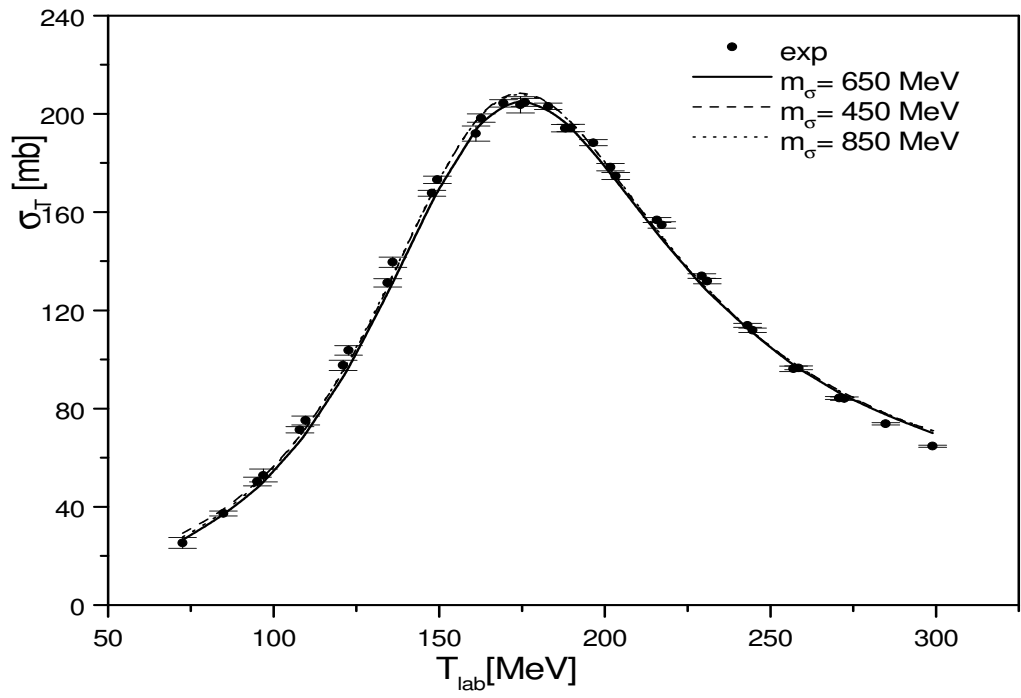


Figure 5

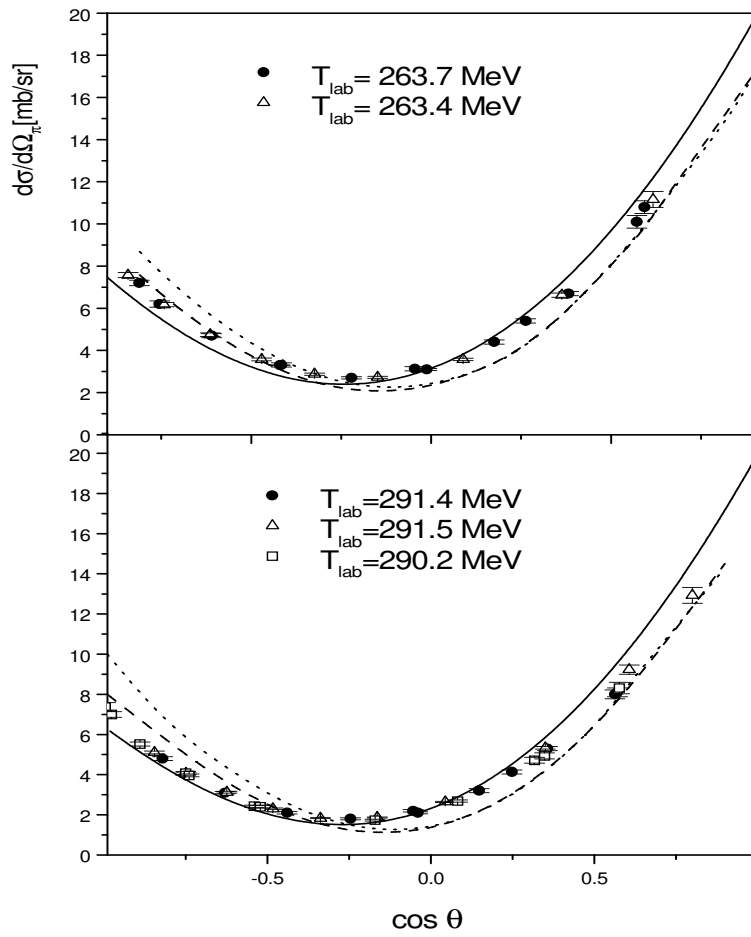


Figure 6

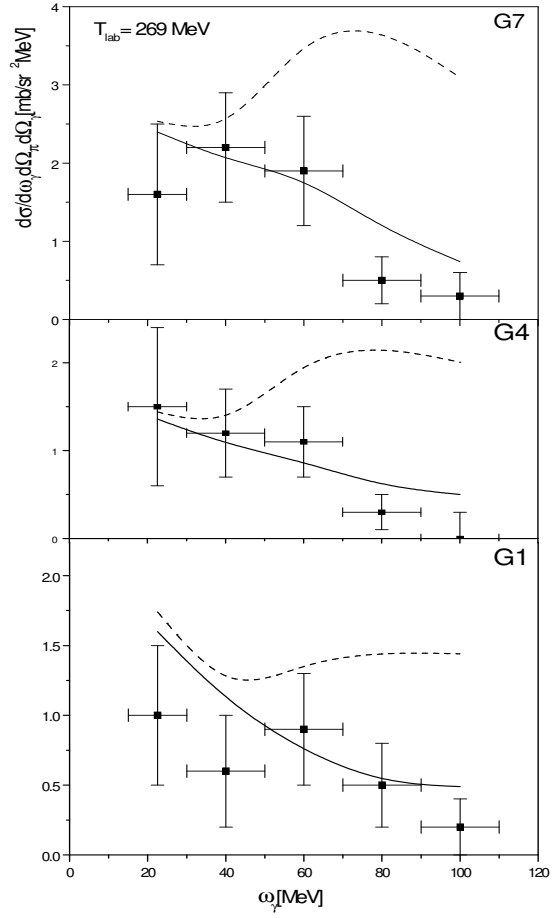


Figure 7

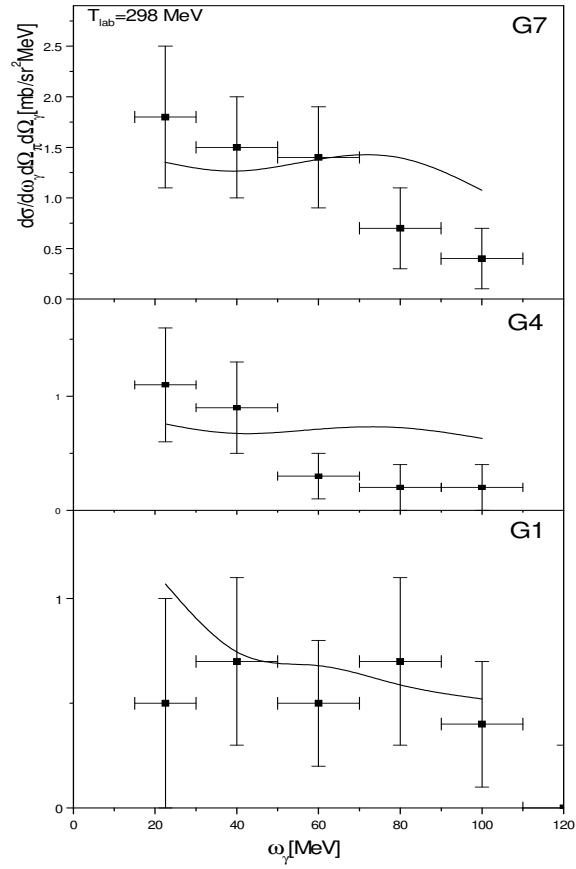


Figure 8

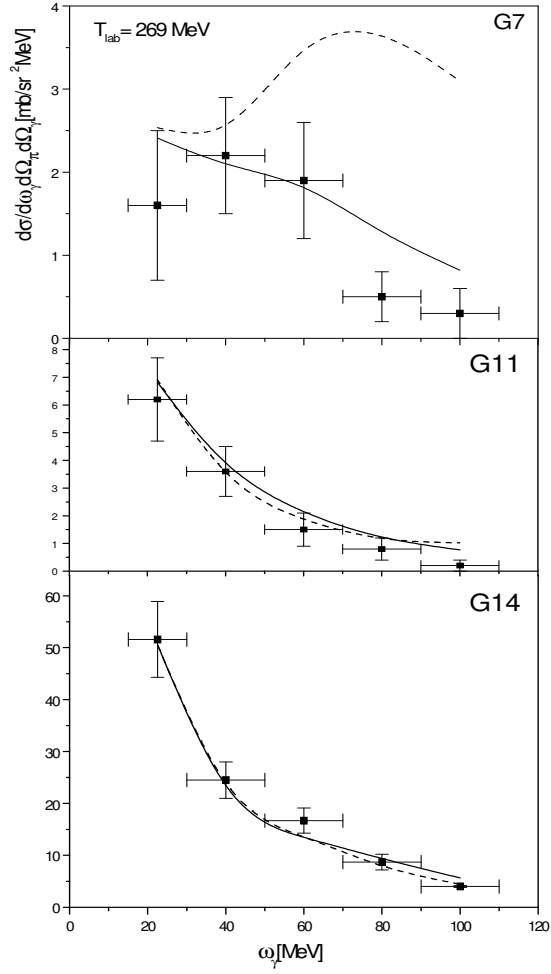


Figure 9

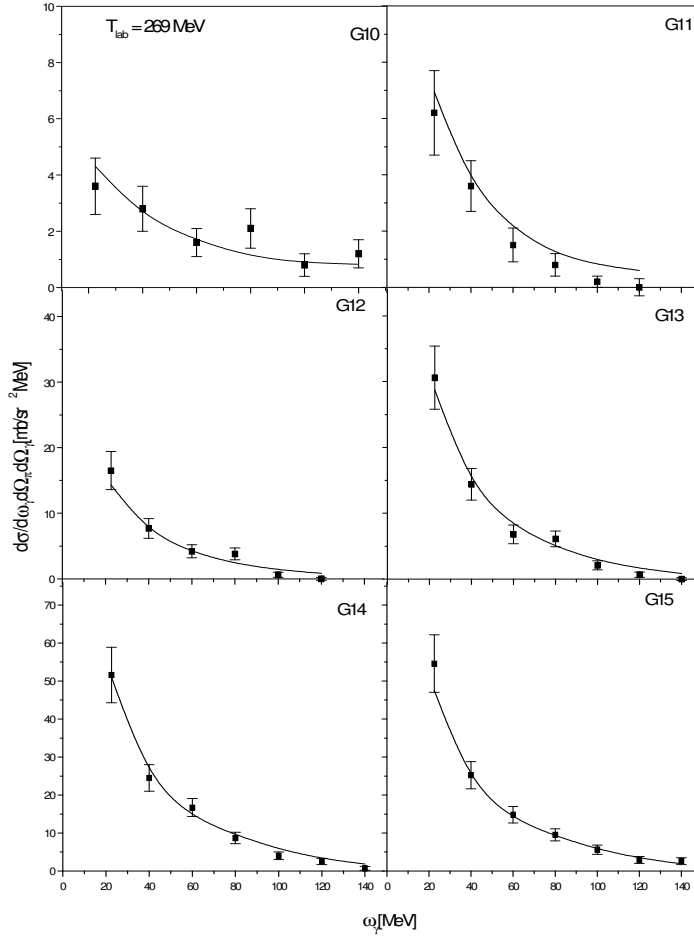


Figure 10

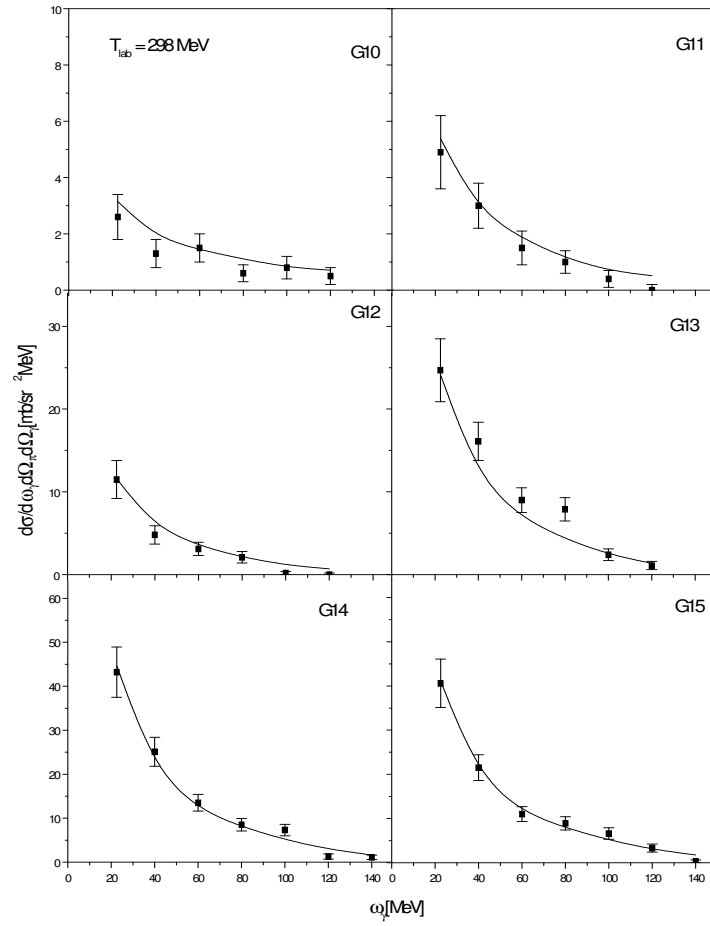


Figure 11